Hindawi Publishing Corporation
Journal of Applied Mathematics
Volume 2012, Article ID 983819, 29 pages
doi:10.1155/2012/983819

Research Article

A Theoretical Approach to Predict the Fatigue Life of Flexible Pipes

José Renato M. de Sousa,[1] Fernando J. M. de Sousa,[1] Marcos Q. de Siqueira,[1] Luís V. S. Sagrilo,[1] and Carlos Alberto D. de Lemos[2]

[1] *Programa de Engenharia Civil (PEC), COPPE/UFRJ, Universidade Federal do Rio de Janeiro, 21945-970 Rio de Janeiro, RJ, Brazil*
[2] *Centro de Pesquisas da Petrobras (CENPES), Cidade Universitária, Quadra 7, Ilha do Fundão, 21949-900 Rio de Janeiro, RJ, Brazil*

Correspondence should be addressed to José Renato M. de Sousa, jrenato@laceo.coppe.ufrj.br

Received 20 January 2012; Accepted 30 April 2012

Academic Editor: Carl M. Larsen

This paper focuses on a theoretical approach to access the fatigue life of flexible pipes. This methodology employs functions that convert forces and moments obtained in time-domain global analyses into stresses in their tensile armors. The stresses are then processed by well-known cycle counting methods, and *S-N* curves are used to evaluate the fatigue damage at several points in the pipe's cross-section. Finally, Palmgren-Miner linear damage hypothesis is assumed in order to calculate the accumulated fatigue damage. A study on the fatigue life of a flexible pipe employing this methodology is presented. The main points addressed in the study are the influence of friction between layers, the effect of the annulus conditions, the importance of evaluating the fatigue life in various points of the pipe's cross-section, and the effect of mean stresses. The results obtained suggest that the friction between layers and the annulus conditions strongly influences the fatigue life of flexible pipes. Moreover, mean stress effects are also significant, and at least half of the wires in each analyzed section of the pipe must be considered in a typical fatigue analysis.

1. Introduction

Unbonded flexible pipes or simply flexible pipes, as in Figure 1, have been employed since the 1970s by the offshore oil and gas industry to transfer oil and gas from offshore wells to floating units (or between floating units), inject water or gas in offshore wells, or control and monitor them. When these pipes are used to transport fluids from the seafloor to production or drilling facilities (or from these facilities to the seafloor), they are called flexible risers.

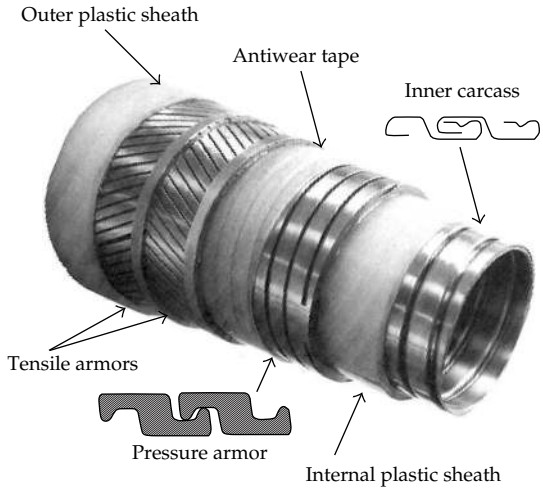

Figure 1: Typical unbonded flexible pipe.

Flexible pipes are composite structures made of several steel and plastic concentric layers designed to meet specific requirements. The polymeric layers work as sealing, insulating, and/or antiwear components, whilst basically three types of metallic layers withstand the imposed structural loads [1]: the *inner carcass* is made from profiled stainless steel strips wound at angles close to 90° (see Figure 1) and mainly resists radial inward forces; the *pressure armor* is usually made from Z-shaped carbon steel wires wound at angles close to 90° (see Figure 1) and supports the system internal pressure and also radial inward forces; *tensile armors* are typically constituted of various rectangular-shaped carbon steel wires laid in two or four layers cross-wound at angles between 20° and 55° that resist tension, torque, and pressure end-cap effects. Aiming at preventing the radial instability of the wires when compressive axial loads act on the pipe, high-strength polymeric tapes, which are usually made of aramid fibers, are wrapped around the outer tensile armor.

These pipes typically operate in water depths up to 2000 m, but recent plans to extend their use to water depths up to 3000 m [2, 3] pose new challenges to their design. Moreover, due to their effectiveness, some of the first flexible pipes installed are still in operation today, but, on the other hand, as operating conditions are being more and more documented, it has been verified that some structures operate in conditions that have proven to be harsher than those adopted in their original designs [4]. Therefore, some flexible pipes are reaching or have already reached their limit service lives, and the decision to keep them in operation (in the same environmental conditions or in less severe ones) or not is concerning operators [5]. In all cases, one of the key issues to be addressed is the fatigue resistance of these structures.

One of the advantages of using flexible pipes instead of rigid steel pipes in offshore systems is the compliance of the formers with the movements of floating facilities and, furthermore, the ability to absorb harsh environmental loads. These characteristics derive from its internal structure in which the individual layers are allowed to slide relative to each other. These movements and environmental loads, however, may provoke high tension and curvature variations in the pipe, which may lead to fatigue failure and/or the wear of the metallic layers. Among all metallic layers of a flexible pipe, its tensile armors are especially prone to fatigue failure [2, 4–10].

Despite the large use of flexible pipes in the offshore oil industry, the determination of their fatigue limits still deserves great attention and, similar to the procedure employed for rigid risers, involves five steps [10]:

(1) collection of environmental loading data and definition of the load case matrix,

(2) global analysis of the riser system, that is, the evaluation of axial forces (tension, as torsion is usually neglected) and bending moments (curvatures) that act on the pipe due to the loads defined in Step 1,

(3) transposition of the tensions and moments determined in the global analysis to theoretical local models devoted to calculate the stresses in each layer of the pipe,

(4) local stress analysis of the pipe focusing on the evaluation of the stresses in the tensile armor wires,

(5) estimation of the fatigue life relying on the stresses calculated in the last step.

This procedure, easily followed in the analysis of rigid steel pipes, implies some difficulties when flexible pipes are analyzed. The computation of stresses is one of the key problems; for rigid pipes, stresses are calculated by simple formulas, and this calculation can be performed directly in the global analyses. For flexible pipes, the evaluation of stresses in their internal layers is not that simple, due to their multilayered structures and complex responses to mechanical loads, mainly when friction between their internal layers is considered. In this way, specific programs have to be employed, and the transposition of tensions and bending moments from the global analyses programs to these programs is needed.

Additionally, many local analyses have to be carried out in order to generate time histories of stresses that are employed to estimate their fatigue lives, but programs devoted to perform local analyses are usually not prepared to carry out thousands (and sometimes millions) of such analyses and store this data for further fatigue assessment.

Finally, according to Grealish et al. [10], traditional approaches to compute the fatigue life of flexible pipes oversimplify key issues associated with the five steps previously indicated. These simplifications are related to the following.

(i) Annulus conditions: the annulus of a flexible pipe is the space between the inner and outer polymeric sheaths that contains the pressure and tensile armors. The characterization of the annulus environment directly influences the choice of the fatigue *S-N* curves to be employed, but fatigue life is normally computed assuming a dry annulus which may lead to unconservative results [8].

(ii) Global analyses: neither the nonlinear bending response of flexible pipes nor bending hysteresis effects, which will be discussed later in this paper, are usually considered. The energy dissipation during loading is normally represented with an equivalent viscous damping.

(iii) Local analyses: the application of response parameters, such as curvature and tension determined from a global analysis, may not be consistent with the manner that the stresses in the wires of the tensile armors are calculated.

(iv) Fatigue methodology: traditional approaches rely on the use of minimum and maximum curvature values that have been derived from regular wave analyses in order to calculate stress ranges. Irregular wave loading, rainflow counting techniques, weather directionality, and frequency domain screening are frequently

neglected or inconsistently employed. Moreover, current methods do not usually account for variations of the dynamic tension, which may be significant in ultradeepwater applications, and also do not generally consider the variation of stresses in the armor wires around the cross-section of the pipe. Finally, locations such as the touchdown zone (TDZ) or bending stiffener areas may not be treated with sufficient rigour.

Therefore, in order to address some of these issues, this paper presents an approach to evaluate the fatigue life of flexible pipes focusing on the calculation of stresses in their tensile armors. This approach employs preestimated functions that convert time histories of forces and moments obtained in global analyses into time histories of stresses in the wires of the tensile armors. The use of these functions speeds up the calculation of stresses, allowing that a great number of cross-sections along the flexible pipe are analyzed with low computational effort. Moreover, these transfer functions also account for load directionality and friction between layers and, consequently, are capable of representing the hysteretic response of flexible pipes subjected to cyclic three-dimensional bending. Finally, time histories of stresses are processed by well-known cycle counting methods and *S-N* curves to evaluate damage at several points in the pipe's cross-section. Palmgren-Miner linear damage hypothesis is assumed in order to calculate the accumulated fatigue damage.

Next, firstly, the proposed approach is presented in detail. After that, various analyses are performed in order to estimate the fatigue life of a flexible riser, and a study is conducted in order to assess the importance of four main aspects in the fatigue response of flexible pipes: the friction between their layers, the annulus conditions, the number of points in the cross-section at which the damage is calculated, and the effect of mean stresses.

2. Theoretical Approach

2.1. Overview

The approach proposed in this paper can be summarized in the following steps.

(1) Environmental loading cases for global analyses are selected from the location scatter diagram.

(2) Global time-domain analyses of the flexible pipe are performed. Time series of tensions and moments at selected locations along the flexible pipe are generated and stored.

(3) A group of coefficients that convert loads imposed to the pipe into stresses in its layers is derived in parallel with (or previous to) the global analyses.

(4) Time series of stresses are automatically generated from the loads evaluated in Step 2 and using the coefficients estimated in Step 3.

(5) Rainflow stress cycle counting for each point of each section of the pipe is performed; fatigue damage is calculated and also accumulated, and, finally, fatigue life is evaluated.

Each of these steps is described in detail next.

2.2. Selection of Environmental Load Cases and Global Analysis

The environmental loads that most influence the analysis and design of offshore structures, such as risers and mooring lines connected to floating units, are waves, wind, and current (see Figure 2). In some specific cases (analysis of TLP tethers, e.g.), tide variation may also be important [11].

From a statistical point of view, these time-dependent environmental loads are random processes. In long-term periods (greater than 1 year), these processes are not stationary; however, for shorter periods (usually 3 h), the parameters that characterize each environmental load present a statistical regularity that allows to consider the stationarity assumption. Each set of environmental parameters for a short-term period of 3 h is called a seastate. A seastate **S** is then defined as [11, 12]

$$\mathbf{S} = \{H_{S_{SW}}, T_{P_{SW}}, \theta_{sw}, H_{S_{SS}}, T_{P_{SS}}, \theta_{ss}, V_w, \theta_w, V_c, \theta_c\}^T, \tag{2.1}$$

where $H_{S_{SW}}$ is the significant height of wind-generated local waves; $T_{P_{SW}}$ is the spectral peak period of local waves, but, depending on the spectra selected to represent the wave, it is also possible to use the zero upcrossing period, T_Z; θ_{sw} is the local wave incidence direction; $H_{S_{SS}}$ is the significant height of swell waves, which are generated by distant storms; $T_{P_{SS}}$ is the spectral peak period of swell waves ($T_{Z_{SS}}$ can also be used); θ_{ss} is the swell incidence direction; the parameters V_w, θ_w, V_c e θ_c represent, respectively, the speed and incidence direction for wind and surface speed and propagation direction for current.

Joint probability distribution functions that include all parameters that characterize a seastate are not usually found in the literature [12]. Environmental parameters are usually described in an individual manner using scatter diagrams. A scatter diagram for local waves, for instance, can be obtained from in situ measurement campaigns [13] in which, for a given incidence direction, θ_w, the measured occurrences, N_i, of waves are defined by (H_s,T_p) pairs. Figure 3 presents an example of a scatter diagram for waves. For current and wind, similar diagrams can be built. Swell waves are in most cases described together with the local waves.

In order to obtain seastates for fatigue analysis from the individual and independent scatter diagrams for waves, wind, and current, a method to combine the environmental loads has to be chosen. This choice can be simplified by recognizing that waves are the most important loads in fatigue calculations [4]. As waves impose dynamic motions to the floating vessel, while current implies only static loads in the risers and offsets in the vessel, and the major wind effects are associated with the mean vessel excursion (offsets), a feasible way to define seastates is to select waves from the scatter diagrams and to combine them with the most probable or 1-year extreme currents and winds in the wave direction, as adopted by de Sousa et al. [14].

Due to the importance of the wave loading in the evaluation of the fatigue life of a riser, its correct numerical simulation is of fundamental importance in the global analyses of flexible pipes. There are basically two ways of representing waves in such analyses: the regular and irregular wave approaches. The regular wave approach is associated with deterministic global riser analyses, whilst the irregular wave approach leads to stochastic global analyses.

In a deterministic global analysis, each pair (H_s,T_p) from the stochastic wave scatter diagram (see Figure 3), which is characterized by significant wave heights, H_s, and spectral peak periods, T_p, or zero upcrossing periods, T_Z, is decomposed into a scatter diagram of individual waves characterized by individual wave heights and periods. Each wave

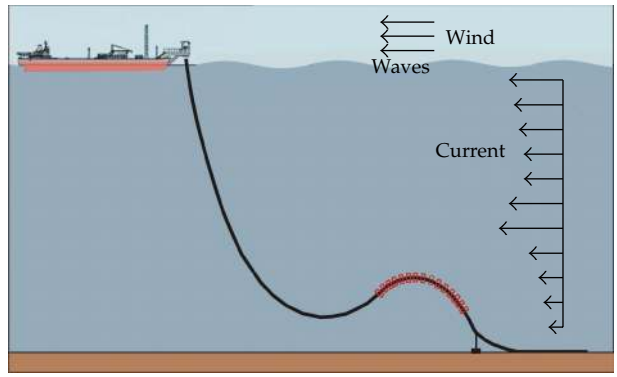

Figure 2: Environmental loads in flexible risers.

Distribution of H_S and T_P for waves approaching from N											
H_s (m) \ T_p (s)		3	4	5	6	7	8	9	10	11	
		4	5	6	7	8	9	10	11	12	
0	0.5	N_1	N_2	N_4	N_7	N_{10}	N_{12}	N_{14}	N_{15}		
0.5	1		N_3	N_5	N_8	N_{11}	N_{13}				
1	1.5			N_6	N_9						
1.5	2										...
2	2.5										
2.5	3										
3	3.5										
⋮											

Figure 3: Example of a scatter diagram for waves.

is then mathematically represented by a sinusoidal function, and, as each global analysis is associated with one regular wave, short simulation times are required (typically of 5 or 6 times the wave period considered in the analysis), and low computational effort is demanded. However, the selection of the individual heights and periods of the waves is a critical aspect of this approach, and the employed methodologies provide values that frequently lead to conservative results [15].

On the other hand, a stochastic global analysis directly considers each seastate of a stochastic scatter diagram, but long simulation times are necessary to stabilize statistical parameters of the response (tensions and moments). These analyses thus demand total simulation times and computational effort much higher than those required in a deterministic analysis, but the loads are more representative of the field environment leading to more realistic results.

The deterministic approach, due to its low computational cost and conservatism, is traditionally used in the computation of the fatigue life of flexible (and rigid) risers. However, recently, stochastic analyses have become more attractive due to the increasing computational capacity and, mainly, the need to reduce the conservatism in fatigue life assessment.

Once the environmental parameters are defined, the whole set of seastates, **S**, is established, and the choice between wave approaches has to be made. Relying on these representations and assumptions, axial forces and bending moments and/or curvatures that act on a flexible pipe in each seastate are usually numerically calculated with finite element (FE) models in which the pipe is modeled with three-dimensional beam

elements; interactions with the seafloor are typically simulated using nonlinear springs, and environmental loads as well as the motions of the floating vessel are represented relying on various mathematical formulations. Different boundary conditions can be assumed, and ancillary components, such as bending stiffeners, can also be incorporated to the model. This type of FE model is called the global model of a flexible pipe, and the associated analysis is named global analysis. Larsen [24] indicate various programs dedicated to perform this task.

The fatigue approach proposed in this work deals with either deterministic or stochastic analyses, but, in performing these analyses, a key point is the generation of time histories of tensions and curvatures, as these time histories are converted to time histories of stresses that are used to compute the fatigue life of flexible pipes. This approach accounts for time variation of the axial forces and bending moments as well as the phasing between these responses thereby reducing the number of simplifying assumptions associated with the transposition of forces and moments, which is discussed next.

2.3. Transposition of Forces and Bending Moments

As mentioned before, the evaluation of stresses in the layers of a flexible pipe is not straightforward, and forces and moments calculated in global analyses programs have to be transposed to programs capable of computing these stresses.

The local analyses of flexible pipes are performed with programs based on one of the various theoretical models available in the literature (see Witz [16] for some examples). These models typically state that

(1) the tensile axial stiffness of a flexible pipe is different from its compressive axial stiffness [17] as well as its clockwise and anticlockwise torsional stiffnesses,

(2) these stiffnesses, for moderate loads, do not vary with the magnitude (positive or negative) of the axial displacement (translation or rotation).

In the design of flexible pipes, axial compression is not desirable as it may cause the excessive bending of these structures or the buckling of their tensile armors wires [17]. As a consequence, in global analyses, the tensile axial stiffness of the pipe and its larger torsional stiffness, which is associated with torsional moments that tighten the outer tensile armor of the pipe [16], are employed, and the axial displacement versus axial load curve is assumed to be linear. Axial forces and torsional moments are therefore calculated according to the hypothesis assumed by the local theoretical models, and these forces can be directly transposed to local programs.

On the other hand, the bending stiffness of the pipe depends on its curvature. Various authors [4, 6, 7, 9, 16, 18–20] describe the bending response of flexible pipes as a stick-slip mechanism which is activated by the contact pressures between layers generated by the axisymmetric loads imposed to the pipe.

For small curvatures, friction between the wires and the adjacent layers prevents their slippage. As a consequence, axial forces are induced in the wires, and these forces are opposed by friction forces with the same magnitude. This leads to a linear bending moment versus curvature relationship with a very high tangent stiffness. This tangent stiffness is usually called no-slip bending stiffness, EI_{ns}.

As curvature increases, interlayer friction is overcome and progressively allows the relative movement of the layers. This slippage reduces the tension increase in the extrados of the pipe and compression decrease in its intrados thereby reducing the tangent stiffness

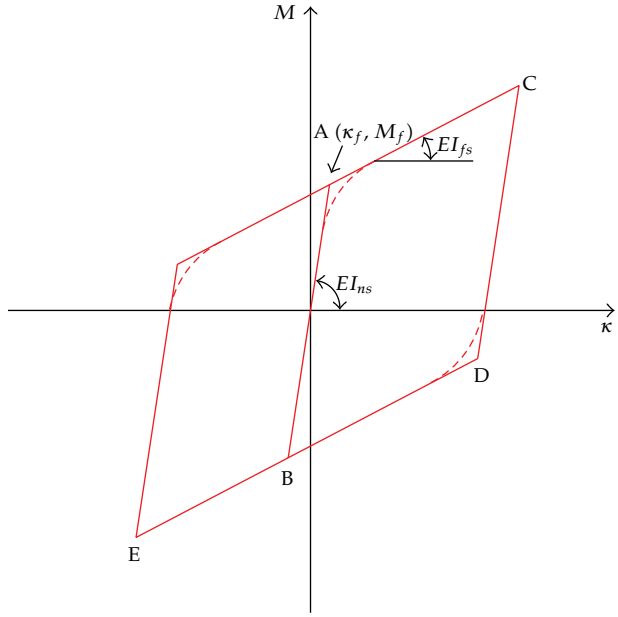

Figure 4: Schematic representation of the hysteretic response of flexible pipes under bending.

of the pipe. This stiffness keeps decreasing until friction forces are fully overcome and the tensile armors are free to slip. At this point, the tangent stiffness reaches a limit value much lower than the no-slip one. This lower limit is called full-slip bending stiffness, EI_{fs}, and is the value usually provided by the flexible pipes manufacturers in their data sheets. Moreover, the curvature at which the interlayer friction is overcome is called critical curvature, κ_f, and the associated bending moment is named internal friction moment, M_f. Figure 4 schematically shows this mechanism.

If a flexible pipe is loaded and unloaded with curvatures lower than the critical value, the bending moment versus curvature relationship is linear (path OAB in Figure 4). However, if the critical curvature is exceeded, the bending moment versus curvature relationship becomes nonlinear and may be approximated by the bilinear curve shown in Figure 4 (path OAC) or by a multilinear curve [4, 9]. If the pipe is unloaded, that is, if the curvature is reversed, initially, the wires are prevented from sliding by the internal friction as axial forces induced by the imposed curvature decrease. When a curvature equivalent to the critical value is exceeded, the wires are loaded again, and a new curvature increment equal to the critical value initiates their relative slide (path CDE in Figure 4). This mechanism leads to a hysteretic loop in which the area between the parallel lines shown in Figure 4 is proportional to the energy dissipation due to friction during the bending of the pipe.

This nonlinear and hysteretic bending response has a substantial impact on the fatigue life computation of flexible pipes mainly due to two aspects [4, 10]:

(1) bending motions imposed to the pipe are reduced as the high preslip bending stiffness sustains small changes of curvature at each curvature reversal, and, moreover, there is a significant energy dissipation associated with higher curvatures,

(2) different stress components and amplitudes may arise in the tensile armor wires during the no-slip and full-slip phases.

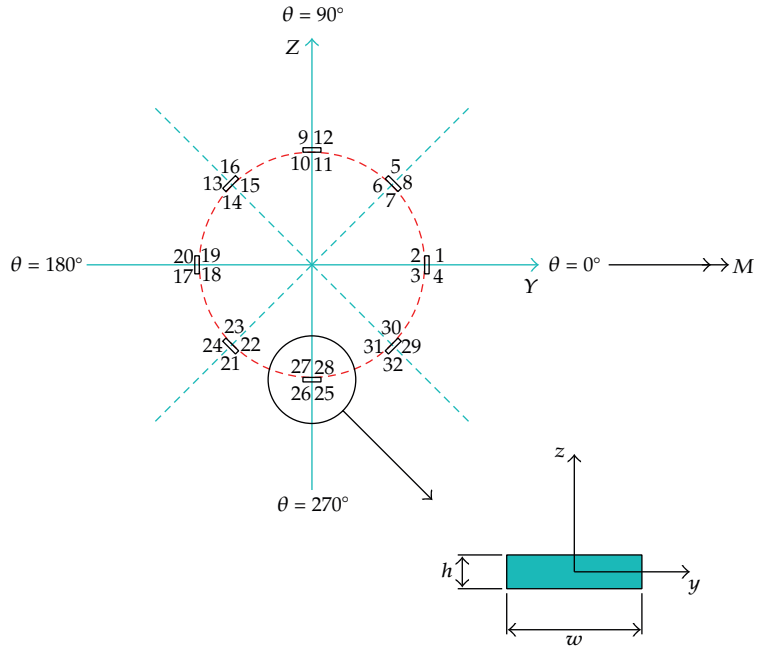

Figure 5: Tensile armor wires in a cross-section of a flexible pipe.

Concerning the second aspect, three different types of stresses arise in the tensile armors wires during bending [6]:

(i) Normal (axial) stresses due to friction, which are uniformly distributed across the section of the wire. These stresses are positive (tensile stresses) in wires located in the extrados of the bent pipe and negative (compressive stresses) in wires located in the intrados of the pipe and also have a limit value associated with the critical curvature.

(ii) Bending stresses due to normal curvature variations, which vary linearly from tension to compression along the thickness of the wire.

(iii) Bending stresses due to transverse (binormal) curvatures, which vary linearly from tension to compression along the width of the wire.

As a result of the helical path of the wires, a sinusoidal distribution along the cross-section of the pipe is typically assumed for these stresses. Considering the bending moment, M, presented in Figure 5, the extreme values for normal friction stresses and normal bending stresses are found at $\theta = 90°$ or $270°$ and $z = \pm h$ (normal bending stresses). On the other hand, the extreme binormal bending stresses are located at $\theta = 0°$ or $180°$ and $z = \pm w$.

Despite its importance in fatigue life computation, the simulation of this nonlinear and hysteretic bending response is not a simple task and is often, conservatively, not considered in global and local analyses of flexible pipes. It is worth mentioning that most programs devoted to perform global analyses have been initially developed to analyze rigid steel pipes and cables or mooring lines. In these structures, the bending moment versus curvature relationship is typically linear, and energy dissipation is mainly due to viscous and hydrodynamic dampings. Therefore, when analyzing flexible pipes with these programs,

the usual approach is to consider a tangent bending stiffness (usually the full slip value, as it is provided by the manufacturers) associated with an equivalent viscous damping, which is set by designers relying on their own practice. Local analyses may be performed considering that the stresses are related to the no-slip phase [6] or the full-slip phase. This approach, however, leads to rather conservative values in the first case or to unconservative values in the second case.

Only in the recent few years, programs capable of considering the described hysteretic response in the global analyses of flexible pipes have been developed [4, 9]. There are also various theoretical approaches to obtain this bending moment versus curvature relationship, but, when compared, these approaches may produce quite different curves. Additionally, the coefficient of friction between layers is usually unknown, and each designer or manufacturer employs values, which frequently vary between 0.07 and 0.20 [7], relying on proprietary experimental or field data or, again, on their own design practice.

In this work, bending moments (or curvatures) calculated either with a linear or nonlinear bending moment versus curvature relationship can be transposed to the local model, but the model always assumes a bilinear and hysteretic relation between stresses and curvatures. If a linear relation is employed in the global analyses, this assumption will reduce the conservatism of the analysis (mainly if the global analyses are performed using the full-slip bending stiffness of the pipe). On the other hand, if a nonlinear relation is employed in the global analyses, this approach will lead to consistent results as long as the friction moment and the critical curvature informed in the bilinear bending moment versus curvature curve are the same of the bending stresses versus curvature curves. The whole procedure is described in detail next.

2.4. Local Analysis

It is common practice in the analysis of flexible pipes to split the total stresses in the wires into two components: stresses associated with axisymmetric loads and stresses induced by the imposed bending moments or curvatures [19]. The same approach is employed in this work, and in what follows the computation of these stresses is outlined.

2.4.1. Stresses due to Axisymmetric Loads

There are several models available in literature devoted to the cross-section (local) analysis of flexible pipes [16], and the vast majority states that the response of these structures to axisymmetric loads, such as tension or axial compression, internal or external pressure, or torsion, is linear and induces only normal (axial) stresses in the wires. Therefore, the application of the superposition principle would be possible, and the normal stress, σ_x^{ax}, in a wire i of a tensile armor of a flexible pipe may be expressed by

$$(\sigma_x^{ax})_i = f_1^{ax} \cdot T + f_2^{ax} \cdot C + f_3^{ax} \cdot P_{\text{int}} + f_4^{ax} \cdot P_{\text{ext}} + f_5^{ax} \cdot T_O, \quad i = 1 \text{ to } n_w, \tag{2.2}$$

where n_w is the number of wires in the layer of the flexible pipe; T, C, P_{int}, P_{ext}, and T_O are, respectively, the tension, axial compression, internal pressure and external pressure, and torsion acting on a section of the pipe; f_j^{ax}, $j = 1$ to 5, are coefficients that transform these acting axisymmetric loads into normal stresses in the wire.

Table 1: Possible contact pressures and stress in the high-strength (HS) tape for a typical unbonded flexible pipe considering different annulus conditions and axisymmetric loading.

Shape	Interface†					Stress (HS tape)	Annulus
	1	2	3	4	5		
1	Contact	Contact	Contact	Contact	Contact	Unloaded	
2	No contact	Contact	Contact	Contact	Contact	Tensioned	
3	No contact	Contact	Contact	Contact	Contact	Unloaded	
4	No contact	Contact	Contact	No contact	Contact	Tensioned	Dry
5	No contact	Contact	Contact	Contact	No contact	Unloaded	
6	No contact	Contact	No contact	No contact	Contact	Tensioned	
7	Contact	Contact	Contact	Contact	No contact	Unloaded	
8	Contact	Contact	Contact	Contact	Contact	Unloaded	
9	No contact	Contact	Contact	Contact	Contact	Tensioned	
10	No contact	Contact	Contact	Contact	Contact	Unloaded	
11	No contact	Contact	Contact	No contact	Contact	Tensioned	
12	No contact	Contact	Contact	Contact	No contact	Unloaded	Flooded
13	Contact	Contact	Contact	Contact	No contact	Unloaded	
14	Contact	No contact	Contact	No contact	Contact	Tensioned	
15	Contact	No contact	Contact	Contact	No contact	Unloaded	
16	Pure external pressure						

† Interface 1: inner carcass and internal plastic sheath; interface 2: internal plastic sheath and pressure armor; interface 3: pressure armor and antiwear tape (or tensile armor); interface 4: pressure armor (or antiwear tape) and internal tensile armor; interface 5: external tensile armor and polymeric layer upon it. In all other interfaces, contact between layers was observed.

In this work, (2.2) was stated relying on various local mechanical analyses carried out using the in-house finite element tool RISERTOOLS [21]. In these analyses, combinations of moderate axisymmetric loads were imposed to a representative set of flexible pipes currently in operation. Both dry and flooded annulus conditions were studied.

In particular, for a typical unbonded flexible pipe with a high-strength tape to prevent axial compression instability of the tensile armor wires, two different types of nonlinearities were observed in the analyses:

(1) loss of contact between some layers of the pipe,

(2) material nonlinearities due to the high-strength tape, which only works when tensioned.

The responses obtained for this type of flexible pipe were grouped in 16 possible deformed shapes, as indicated in Table 1. Each deformed shape is associated with different load levels, which are outlined in Table 2. These analyses also pointed out that (2.2) is only valid if the proper choice of contact conditions and stress in the high-strength tape are assumed. Hence, for the correct calculation of the stresses in the tensile armors of the flexible pipe, it is firstly necessary to identify which deformed shape is generated by the axisymmetric loads applied.

Therefore, for each of the possible deformed shapes, five analyses, which effectively produce the assumed contact and stress conditions presented in Table 1, are performed, and coefficients, f^{ax}, related to the contact pressures, stress in the high-strength tape and stresses in the tensile armors wires are determined using (2.2) (in case of evaluating the

Table 2: Load characteristics for each possible deformed shape of a typical unbonded flexible pipe considering different annulus conditions and axisymmetric loading.

Shape	Load characteristics†	Annulus
1	High tension (no axial compression), low internal pressure, high external pressure, moderate torsion	Dry
2	Low tension or axial compression, high internal pressure, low external pressure, low torsion	
3	High tension, high internal pressure, moderate external pressures (internal pressure higher than external pressure), low torsion	
4	High axial compression (no tension), high internal pressure, low external pressure, low torsion	
5	High tension and internal pressure, no external pressure, moderate torsion	
6	High axial compression, low internal and external pressures, low torsion	
7	High tension and low internal and external pressures, low torsion	
8	Analogous to shape 1	Flooded
9	Analogous to shape 2	
10	Analogous to shape 3	
11	Analogous to shape 4	
12	Analogous to shape 5	
13	Analogous to shape 7	
14	High axial compression, no internal pressure, high external pressure, low torsion	
15	High tension, no internal pressure, high external pressure, low torsion	
16	Pure external pressure	

† The fundamental aspect is to maintain the proportionality between the loads. Therefore, a high load value could be its limit for the studied flexible pipe; a low value may be, for instance, 1% of the limit value, and a moderate value could be 50% of the limit value.

contact pressures, consider the contact pressure variable instead of the normal stress in the left side of the equation). Then, for a given set of axisymmetric loads, each of the possible deformed configurations is verified; that is, the contact pressures in each interface and the stress in the high-strength tape, induced by these loads are calculated with (2.2) considering the coefficients related to each of these configurations. The deformed shape that does not violate the associated hypotheses is the valid one. Finally, (2.2) is again applied to determine the stresses in the tensile armors considering the coefficients linked to the chosen deformed condition.

This methodology allows the computation of the stresses in the armors with few simple operations and low computational effort. As a consequence, in a typical fatigue analysis, the stresses induced in the armors may be evaluated at each time step of all considered time histories.

2.4.2. Stresses due to Bending Moments

The computation of the stresses due to the bending of the pipe is based on a vector hysteresis model. In this model, an in-plane stress versus curvature relationship, which has to be previously defined, is extended in order to account for the three-dimensional bending of the pipe.

The model relies on a set of equations proposed by Fylling and Bech [22] to simulate the nonlinear and hysteretic bending response of flexible pipes. As the stresses induced by bending in the wires of the tensile armors are directly related to the imposed curvature, the same approach is used here to calculate these stresses.

If a curvature increment $\Delta\boldsymbol{\kappa} = (\Delta\kappa_x, \Delta\kappa_y)$ is imposed to a flexible pipe at a deformed configuration 1, with total curvature $\boldsymbol{\kappa}_1 = (\kappa_{x1}, \kappa_{y1})$, leading to a deformed configuration 2, the total curvature $\boldsymbol{\kappa}_2 = (\kappa_{x2}, \kappa_{y2})$ at configuration 2 is given by

$$\boldsymbol{\kappa}_2 = \boldsymbol{\kappa}_1 + \Delta\boldsymbol{\kappa}. \tag{2.3}$$

Fylling and Bech [22] state that in all deformed configurations, the total curvature acting on a flexible pipe can be split in two parts: the first one, $\boldsymbol{\kappa}_f = (\kappa_{fy}, \kappa_{fz})$, is attributed to the phase in which no slippage occurs between layers; the second one, $\boldsymbol{\kappa}_e = (\kappa_{ey}, \kappa_{ez})$, is related to the phase in which the layers are free to slip. Therefore, the total curvature imposed to the pipe can be written as

$$\boldsymbol{\kappa} = \boldsymbol{\kappa}_e + \boldsymbol{\kappa}_f. \tag{2.4}$$

Moreover, by hypothesis, the relative slide of the wires starts when the total curvature modulus exceeds the internal friction curvature, $\boldsymbol{\kappa}_f$, and the direction of the friction moment depends on both the curvature increment and on the actual friction force level and direction. Assuming that the stress versus curvature can be expressed by a bilinear curve, the amplitudes of the normal and transverse stresses in the wires of a tensile armor may be given by

$$\sigma_{x2}^{n,y} = \begin{cases} f_2^b \cdot \kappa_{ey1} + f_1^b \cdot \Delta\kappa_y^*, & \text{if } p \le 1, \\ f_2^b \cdot \kappa_{ey1} + \dfrac{p-1}{p} \cdot f_2^b \cdot \Delta\kappa_y^* + \dfrac{1}{p} \cdot f_1^b \cdot \Delta\kappa_y^*, & \text{if } p > 1, \end{cases} \tag{2.5}$$

$$\sigma_{x2}^{n,z} = \begin{cases} f_2^b \cdot \kappa_{ez1} + f_1^b \cdot \Delta\kappa_z^*, & \text{if } p \le 1, \\ f_2^b \cdot \kappa_{ez1} + \dfrac{p-1}{p} \cdot f_2^b \cdot \Delta\kappa_z^* + \dfrac{1}{p} \cdot f_1^b \cdot \Delta\kappa_z^*, & \text{if } p > 1, \end{cases} \tag{2.6}$$

$$\sigma_{x2}^{t,y} = \begin{cases} f_4^b \cdot \kappa_{ey1} + f_3^b \cdot \Delta\kappa_y^*, & \text{if } p \le 1, \\ f_4^b \cdot \kappa_{ey1} + \dfrac{p-1}{p} \cdot f_4^b \cdot \Delta\kappa_y^* + \dfrac{1}{p} \cdot f_3^b \cdot \Delta\kappa_y^*, & \text{if } p > 1, \end{cases} \tag{2.7}$$

$$\sigma_{x2}^{t,z} = \begin{cases} f_4^b \cdot \kappa_{ez1} + f_3^b \cdot \Delta\kappa_z^*, & \text{if } p \le 1, \\ f_4^b \cdot \kappa_{ez1} + \dfrac{p-1}{p} \cdot f_4^b \cdot \Delta\kappa_z^* + \dfrac{1}{p} \cdot f_3^b \cdot \Delta\kappa_z^*, & \text{if } p > 1, \end{cases} \tag{2.8}$$

where $\sigma_{x2}^{n,y}$ and $\sigma_{x2}^{n,z}$ are the amplitudes of the normal bending stresses about directions Y and Z (see Figure 5) at the deformed configuration 2, while $\sigma_{x2}^{t,y}$ and $\sigma_{x2}^{t,z}$ are the amplitudes of

the binormal bending stresses about directions Y and Z (see Figure 5) at the same deformed configuration; p and $\Delta\boldsymbol{\kappa}^* = (\Delta\kappa_x^*, \Delta\kappa_y^*)$ are given by

$$p = \frac{1}{\kappa_f} \cdot |\boldsymbol{\Delta\kappa} + \boldsymbol{\kappa}_{\mathbf{f1}}|, \tag{2.9}$$

$$\Delta\boldsymbol{\kappa}^* = \boldsymbol{\Delta\kappa} + \boldsymbol{\kappa}_{\mathbf{f1}}. \tag{2.10}$$

In (2.8) and (2.9), $\boldsymbol{\kappa}_{\mathbf{f1}}$ is the curvature vector associated with the friction phase at the deformed configuration 1; κ_f is the internal friction curvature, which may be expressed in the form

$$\kappa_f = \left| f_5^b \cdot P_{ci} + f_6^b \cdot P_{ce} \right|, \tag{2.11}$$

and P_{ci} and P_{ce} are the contact pressures on the internal and external surfaces of the considered tensile armor layer.

Coefficients f_j^b, $j = 1$ to 6, can be obtained from any of the local analytical or numerical models devoted to the prediction of stresses due to the bending of flexible pipes. In this work, it is assumed that, during the no-slip phase, the deformed shape of the wires follows a loxodromic curve, whilst in the full-slip phase, the deformed shape corresponds to a geodesic curve. Therefore, expressions proposed by Saevik [18] and Estrier [23] are adopted, and coefficients f_j^b are thus given by

$$\begin{aligned}
f_1^b &= \frac{E \cdot h}{2} \cdot \cos^4(\alpha), \\
f_2^b &= \frac{3 \cdot E \cdot h}{2} \cdot \cos^2(\alpha), \\
f_3^b &= \frac{E \cdot w}{2} \cdot \cos(\alpha) \cdot \left[1 + \sin^2(\alpha)\right], \\
f_4^b &= 0, \\
f_5^b &= \frac{\pi^2 \cdot \mu_{\text{inf}}}{4 \cdot E \cdot h \cdot \cos^2(\alpha) \cdot \sin(\alpha)}, \\
f_6^b &= \frac{\pi^2 \cdot \mu_{\text{sup}}}{4 \cdot E \cdot h \cdot \cos^2(\alpha) \cdot \sin(\alpha)},
\end{aligned} \tag{2.12}$$

where h and w are the height and width of the wires, E is their Young modulus, α is the lay angle of the wires, and μ_{inf} and μ_{sup} are the friction coefficients of the wires with the inner and

outer surrounding layers. The friction stress amplitudes about Y and Z axis (see Figure 5), $\sigma_x^{at,y}$ and $\sigma_x^{at,z}$, are given by

$$\left(\sigma_x^{at,y}\right)_i = \begin{cases} \left|\sigma_{\max}^{at}\right| \cdot \dfrac{\Delta\kappa_y^*}{\kappa_f}, & \text{if } p \le 1, \\ \left|\sigma_{\max}^{at}\right| \cdot \dfrac{\Delta\kappa_y^*}{\kappa_f} \cdot \dfrac{1}{p}, & \text{if } p > 1, \end{cases}$$
$$\left(\sigma_x^{at,z}\right)_i = \begin{cases} \left|\sigma_{\max}^{at}\right| \cdot \dfrac{\Delta\kappa_z^*}{\kappa_f}, & \text{if } p \le 1, \\ \left|\sigma_{\max}^{at}\right| \cdot \dfrac{\Delta\kappa_z^*}{\kappa_f} \cdot \dfrac{1}{p}, & \text{if } p > 1, \end{cases} \tag{2.13}$$

where $i = 1, n_w$ and the maximum friction stress amplitude, $\sigma_{\max}^{at}$, is given by

$$\sigma_{\max}^{at} = f_7^b \cdot \sum(\mu \cdot P_c). \tag{2.14}$$

In (2.14), $\sum(\mu \cdot P_c)$ are the total friction forces that act on the wires, and f_7^b is a stress coefficient, which may be expressed as [23]

$$f_7^b = \frac{2 \cdot \pi \cdot r^2}{n_w} \cdot \frac{1}{w \cdot h} \cdot \frac{1}{\tan(\alpha)}, \tag{2.15}$$

where r is the mean radius of the tensile armor layer.

Finally, considering (2.3) to (2.15), the stresses due to bending in a tensile armor wire located at an angular position θ (see Figure 5) are given by

$$\sigma_x^n(\theta_i) = \sigma_{x2}^{n,y} \cdot \sin(\theta_i) + \sigma_{x2}^{n,z} \cdot \cos(\theta_i), \tag{2.16}$$

$$\sigma_x^t(\theta_i) = \sigma_{x2}^{t,y} \cdot \cos(\theta_i) + \sigma_{x2}^{t,z} \cdot \sin(\theta_i), \tag{2.17}$$

$$\sigma_x^{at,y}(\theta_i) = \left(\sigma_x^{at,y}\right)_i \cdot \sin(\theta_i) + \left(\sigma_x^{at,z}\right)_i \cdot \cos(\theta_i), \tag{2.18}$$

where $i = 1, n_w$ and $\theta_i = (i-1) \cdot 360^\circ / n_w$.

2.5. Total Stresses in the Wires of the Tensile Armors

In this work, the time series of stresses for each load case are generated from the tension and moments time series calculated in the global analysis using (2.2) to (2.18).

The first time step of the time series of tension and curvatures corresponds to the results from the static analysis. From these results, the static stresses are determined considering the methodology previously described. The critical curvature estimated for this step is kept throughout the whole dynamic analysis for each load case.

Dynamic axisymmetric stresses are calculated using (2.2) and the appropriate set of coefficients f^{ax}, that is, coefficients related to the deformed shape generated by the combination of the axisymmetric loads in each time step.

Bending stresses are calculated by maintaining the critical curvature of each static analysis and considering that the static configuration is the unstressed one. The stress variations, which correspond to the dynamic stresses, are obtained by considering the variation of the curvature related to the static stresses. It means that the total curvatures in the dynamic analyses are the difference between the dynamic curvatures calculated in the global analyses and the static curvature. Hence, the stresses at each corner of a tensile armor wire may be expressed by the following formulas.

Corner i (see Figure 5):

$$\sigma_x^{\mathrm{tot}}(\theta_i) = \left[(\sigma_x^{ax})_i + \sigma_x^{at}(\theta_i) - \sigma_x^{n}(\theta_i) + \sigma_x^{t}(\theta_i)\right]_{\mathrm{sta}} + \left[(\Delta\sigma_x^{ax})_i + \Delta\sigma_x^{at}(\theta_i) - \Delta\sigma_x^{n}(\theta_i) + \Delta\sigma_x^{t}(\theta_i)\right]_{\mathrm{dyn}}. \tag{2.19}$$

Corner 2i (see Figure 5):

$$\sigma_x^{\mathrm{tot}}(\theta_i) = \left[(\sigma_x^{ax})_i + \sigma_x^{at}(\theta_i) + \sigma_x^{n}(\theta_i) + \sigma_x^{t}(\theta_i)\right]_{\mathrm{sta}} + \left[(\Delta\sigma_x^{ax})_i + \Delta\sigma_x^{at}(\theta_i) + \Delta\sigma_x^{n}(\theta_i) + \Delta\sigma_x^{t}(\theta_i)\right]_{\mathrm{dyn}}. \tag{2.20}$$

Corner 3i (see Figure 5):

$$\sigma_x^{t}(\theta_i) = \left[(\sigma_x^{ax})_i + \sigma_x^{at}(\theta_i) + \sigma_x^{n}(\theta_i) - \sigma_x^{b}(\theta_i)\right]_{\mathrm{sta}} + \left[(\Delta\sigma_x^{ax})_i + \Delta\sigma_x^{at}(\theta_i) + \Delta\sigma_x^{n}(\theta_i) - \Delta\sigma_x^{b}(\theta_i)\right]_{\mathrm{dyn}}. \tag{2.21}$$

Corner 4i (see Figure 5):

$$\sigma_x^{t}(\theta_i) = \left[(\sigma_x^{ax})_i + \sigma_x^{at}(\theta_i) - \sigma_x^{n}(\theta_i) - \sigma_x^{b}(\theta_i)\right]_{\mathrm{sta}} + \left[(\Delta\sigma_x^{ax})_i + \Delta\sigma_x^{at}(\theta_i) - \Delta\sigma_x^{n}(\theta_i) - \Delta\sigma_x^{b}(\theta_i)\right]_{\mathrm{dyn}}. \tag{2.22}$$

where $i = 1$ to n_w, subscripts sta and dyn refer, respectively, to the static and dynamic components of the calculated stresses, and Δ corresponds to the variation of the stress with respect to the static analysis.

2.6. Fatigue Damage and Fatigue Life Computation

The approach proposed in this work computes stresses (and fatigue damage) at several points in the pipe's cross-section and for each of the environmental load cases considered. The number of stress cycles in each of these time series is counted using the rainflow technique, and the fatigue damage associated with each stress cycle is evaluated using *S-N* curves. It is worth mentioning that the choice of the *S-N* curve is linked to the annulus condition of the pipe, and this condition (dry or flooded) should also be taken into account in the stress calculation, as previously stated.

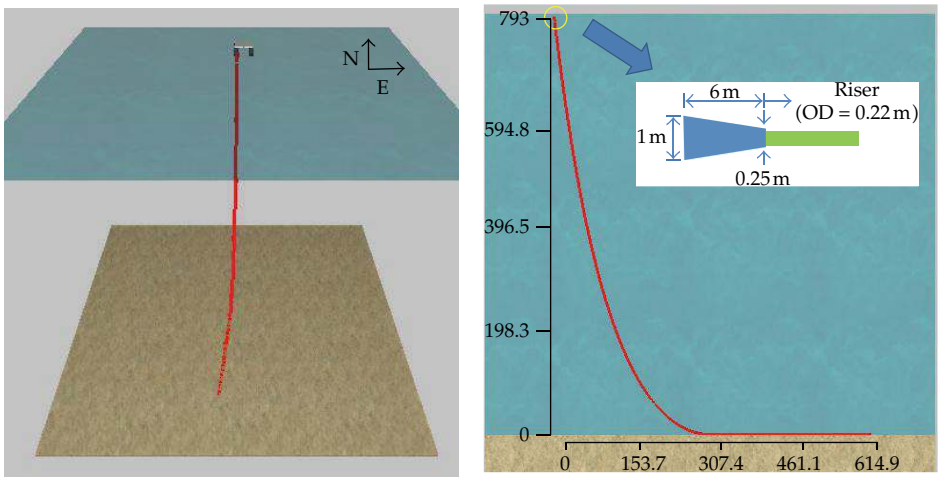

(a) (b)

Figure 6: General overview of the studied flexible pipe: (a) perspective and (b) lateral view.

Finally, fatigue damage is accumulated assuming that the Palmgren-Miner rule is valid, and the fatigue life in each section is represented by the minimum value obtained for all processed points. It is also worth mentioning that mean stress effects may be addressed using the well-known Goodman correction factor.

2.7. Implementation

As mentioned before, the global loads that act on the pipe may be assessed with one of the various programs devoted to perform this task (see Larsen [24] for a general overview of these programs). Furthermore, coefficients employed in the local analysis are here determined with the in-house FE tool RISERTOOLS [21], but any of the local models available in the literature (see Witz [16] for some examples) could also be used.

In order to speed up the calculation of stresses and evaluation of the fatigue life, a specific tool called FADFLEX was developed. FADFLEX performs the transposition from the global to the local model and computes stresses at each desired point along the flexible pipe. Moreover, stress cycles are counted by this program, and fatigue damage is calculated. Finally, the program estimates the fatigue life of the flexible pipe.

3. Case Study

3.1. Description

As an example of the proposed methodology for fatigue evaluation of flexible pipes, a 6" oil production riser connected to a FPSO (Floating Production, Storage and Offloading) vessel was selected. The riser is in a free hanging configuration (7° top angle, 185° azimuth) in a water depth of 800 m. It has 8 layers including two tensile armors. The inner tensile armor has 56 wires, whilst the outer tensile armor has 58 wires. All wires are 3 mm in height and 9 mm in width. The axial stiffness of the pipe is 357 MNm/m, and its full slip bending stiffness equals 12.8 kNm^2. Figure 6 shows a general layout of the pipe configuration and a detail of

the bending stiffener positioned at the connection with the FPSO. This stiffener prevents the excessive bending of the pipe in the top region.

The seastates employed in the fatigue analysis were obtained from Campos Basin (offshore Brazil) metocean data [25]. Sixty load cases composed by irregular waves, currents, and offsets were analyzed, as wind does not generate forces directly on the riser.

All environmental loads were supposed aligned (8 directions). Scatter diagrams similar to the one presented in Figure 3 were employed to select the waves. However, selecting all possible waves would imply the analysis of more than 1000 seastates, and, consequently, a simplified approach was required. Aiming at reducing the number of seastates, for each direction and period range, only one wave, composed by the mean period and the highest associated wave height in the scatter diagram, was selected; the occurrence frequency adopted for these waves was computed based on the total number waves in the same period range/direction.

For each direction, the currents selected to compose each load case were the 1-year extreme currents. The offsets were estimated supposing a value equivalent to 10% of the water depth associated with the largest wave in Campos Basin (≈8 m) and linearity between offsets and wave heights.

All global time-domain analyses were performed by the in-house tool ANFLEX [26] considering an irregular wave and a simulation length of 1200 s.

In order to obtain the coefficients f^{ax} and f^{b}, 38 local analyses were performed with RISERTOOLS [21] to calculate the coefficients related to the axisymmetric response of the pipe, and (2.12) was used to calculate the coefficients related to the bending response.

Considering the objectives of the work, which are to illustrate the use of the proposed approach and to evaluate the effect of some parameters in the fatigue response of a flexible pipe, the base case assumed the following premises.

(1) The annulus of the pipe is flooded with seawater.

(2) A friction coefficient of 0.10 between the layers of the pipe is initially considered.

(3) Mean stresses effects are accounted for by the Goodman correction factor.

(4) The *S-N* curve employed in the fatigue analysis was the one established by DNV [27] for high strength steel ($m = 4.7, \log(A) = 17.446$), which considers the presence of seawater.

(5) All wires of the tensile armors had their fatigue lives calculated.

Next, firstly, the fatigue life of the 6″ flexible riser considering the conditions previously described is computed. After that, relying on the results obtained, the effect of each of the following four parameters on the fatigue response of the pipe is evaluated: friction between layers, annulus conditions, mean stress effects, and number of points considered in each cross-section.

3.2. Base Case

Figure 7 presents the variation of the fatigue life along the tensile armors of the flexible pipe and indicates two critical regions: the top connection (inside the bend stiffener) and the touchdown zone (TDZ), which are the regions presenting more pronounced bending effects. Out of these regions, the fatigue life is directly related to the variation of the axisymmetric loads, as bending moments are negligible. Furthermore, this figure also indicates that the

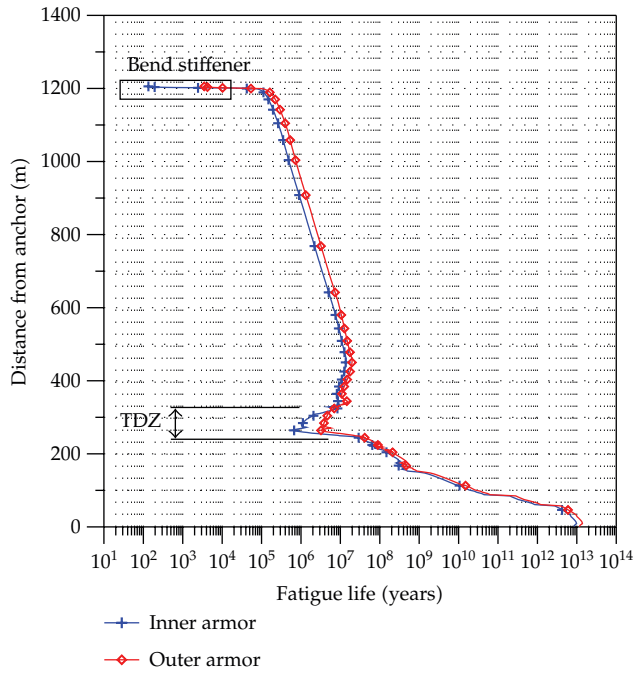

Figure 7: Fatigue life along the flexible pipe: base case.

fatigue lives predicted for the wires of the inner and outer tensile armors are relatively close, but lower values are observed in the inner armor in all cross-sections of the pipe and, especially, in the cross-sections inside the bend stiffener. As a consequence, the inner armor governs the fatigue response of the flexible riser.

The cross-section with the lowest fatigue life is located inside the bend stiffener. Figure 8 details the variation of the fatigue life along the wires of the inner and outer tensile armors in this cross-section. This figure indicates that the fatigue life considerably varies along the wires in both layers, and, therefore, the number of wires to be monitored during a fatigue analysis is an important parameter. Figure 8 also shows that the lowest fatigue life in the inner tensile armor occurs in wire 10 and is equal to 135 years, whilst the lowest fatigue life in the outer armor occurs in wire 12 and is equal to 3511 years. These wires are situated approximately at the same angular position (θ).

Figure 9 presents the time series of stresses at the corner with the highest damage in wire 10 of the inner armor, and Figure 10 presents the time series of stresses in wire 12 of the outer armor. These time series of stresses were generated with the environmental load case that induced the highest fatigue damage in these wires.

Figure 9 indicates stresses amplitudes of 52 MPa (axisymmetric stresses), 79 MPa (normal friction stresses), 25 MPa (normal bending stresses), and 12 MPa (transverse bending stresses). Figure 10 indicates amplitudes of 50 MPa (axisymmetric stresses), 27 MPa (normal friction stresses), 18 MPa (normal bending stresses), and 5 MPa (transverse bending stresses). These results indicate that the higher contributions to the stress variation are due to the axisymmetric stresses, which are induced by tension variations, and, mainly, the normal friction stresses. Moreover, as the stress amplitudes are higher in the inner armor, fatigue lives are lower in this armor, and it governs the fatigue response of the riser.

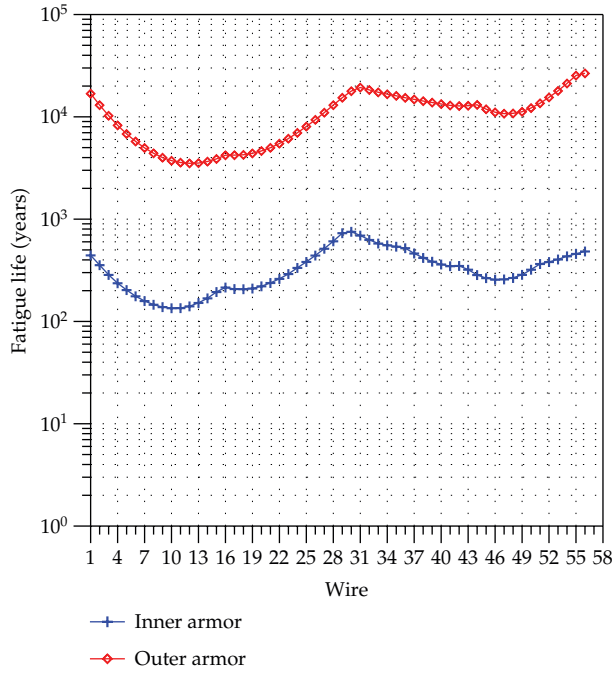

Figure 8: Fatigue life along the critical section: base case.

3.3. Effect of Different Friction Coefficients

In order to evaluate the effect of different friction coefficients on the fatigue life prediction of the flexible riser, five different values were considered: 0.00 (no friction), 0.05, 0.10 (base case), 0.20, infinite (fully bonded response). Figure 10 shows the variation of the fatigue life in the inner armor along the flexible riser, and Figure 11 shows variation of the fatigue life in the inner armor along the flexible riser, and Figure 12 shows the same variation, but in the outer armor. Table 3 summarizes the critical values.

These figures and tables indicate that the choice of the friction coefficient is a key aspect in predicting the fatigue life of a flexible riser. In the analysis with no friction, local and global models assume the same hypotheses, and no hysteresis is expected to occur in the riser response. However, no friction stresses are induced, and, as mentioned before, these stresses largely contribute to the fatigue damage on the riser. Therefore, high and unconservative values for the fatigue lives are predicted in both layers. The assumption of a friction coefficient of 0.05 reduces the fatigue life of the riser in 1/75. It is interesting to observe that this reduction is obtained in the inner armor, but in the outer armor the reduction is of about 1/7, as friction stresses are lower in this layer. The increase of the friction coefficients keeps reducing the fatigue life until a limit value of 19 years is reached in both layers for infinite friction.

It is worth mentioning that, if infinite friction is assumed, the global analysis should be performed considering the no-slip bending stiffness, and, consequently, much lower curvatures would be obtained. Hence, the values obtained with infinite friction maximize the stresses in the wires, and the hypothesis of full slip bending stiffness in the global analyses maximizes the curvatures calculated leading to quite conservative values for the fatigue lives.

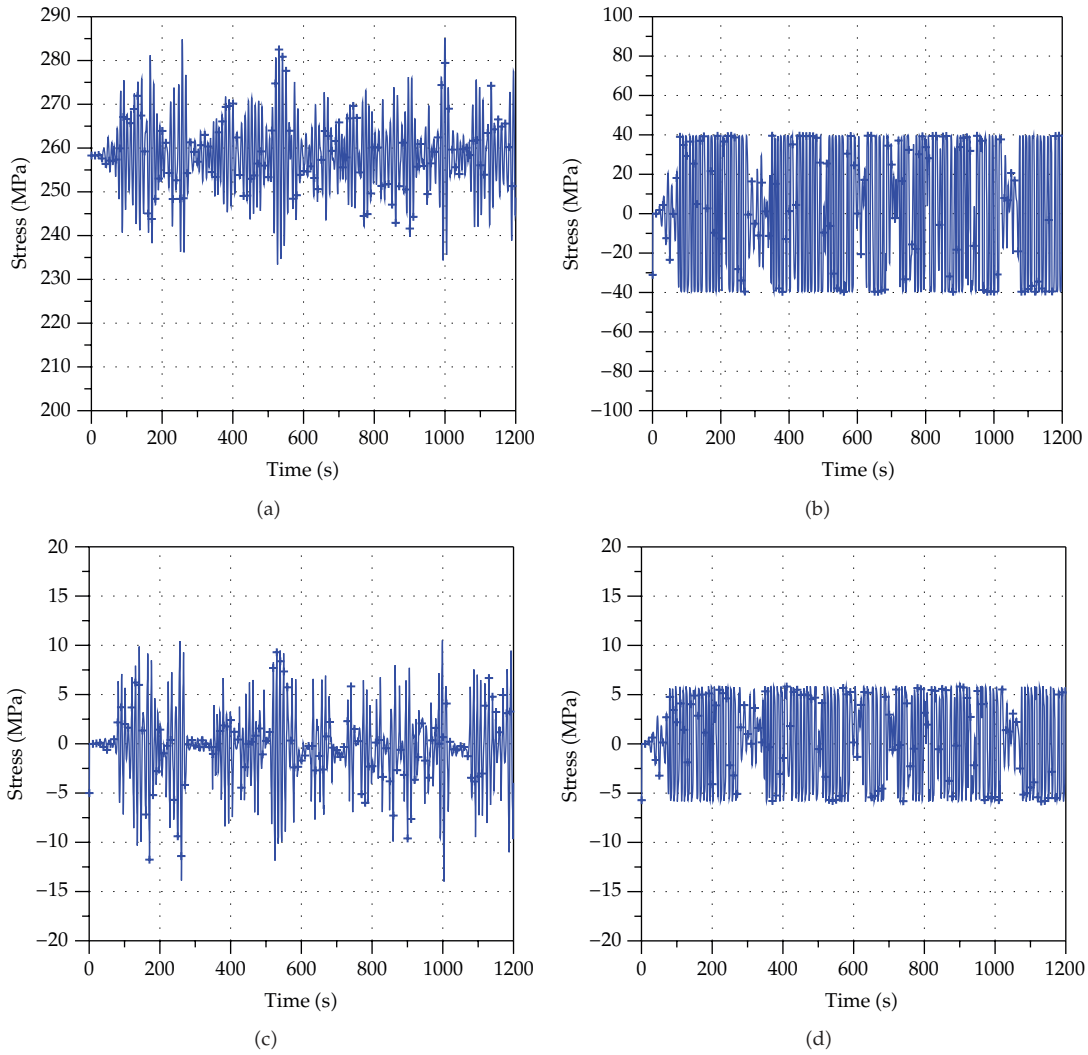

Figure 9: Time histories of stresses in wire 10 (corner with the highest fatigue damage) of the inner tensile armor: (a) axisymmetric stresses; (b) normal friction stresses; (c) normal bending stresses; (d) transverse bending stresses.

A possible approach, consequently, would be the choice of a lower friction coefficient, such as 0.05 or 0.10, and the use of the full-slip bending stiffness in the global analysis to ensure some conservatism in the fatigue analysis.

3.4. Effect of Different Annulus Conditions

In the previous analyses, the annulus of the pipe was considered to be flooded with seawater. Here, the response of the riser with a dry annulus is assessed considering the base case conditions and an *S-N* curve for high-strength steel without the presence of seawater [27].

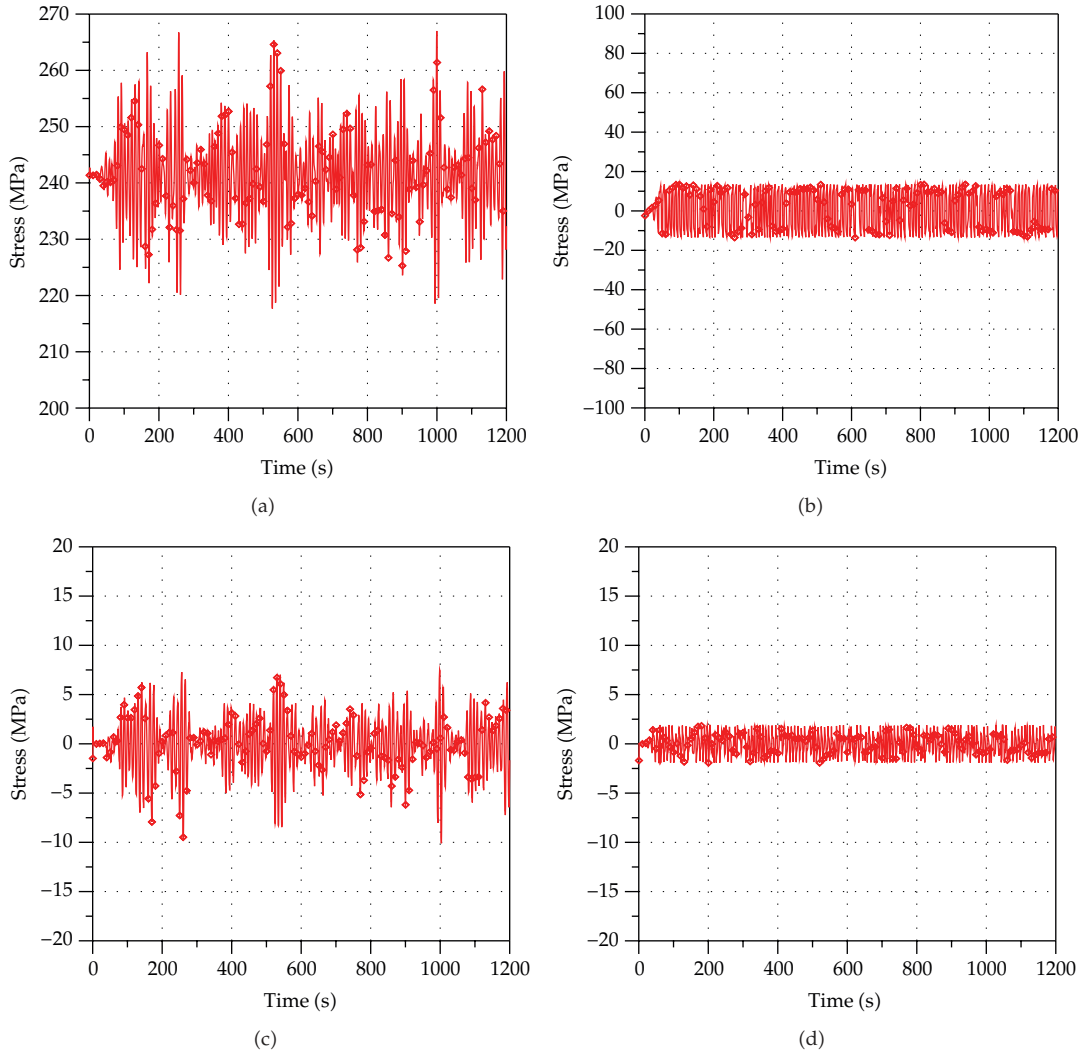

Figure 10: Time histories of stresses in wire 12 (corner with the highest fatigue damage) of the outer tensile armor: (a) axisymmetric stresses; (b) normal friction stresses; (c) normal bending stresses; (d) transverse bending stresses.

This curve is similar to the one used in the analysis with flooded annulus, but there is a fatigue threshold for a stress of 235 MPa.

When the annulus of the pipe is dry, the external pressure acts on its outer sheath leading to high contact pressures between the tensile armors and the adjacent layers in sections located in the TDZ, and, consequently, no slippage between layers occurs in these sections. Therefore, in order to make consistent global and local analyses, the full-slip bending stiffness employed in the global analyses was replaced by the no-slip value in the cross-sections located in the TDZ. In this work, the no-slip bending stiffness, EI_{ns}, proposedby

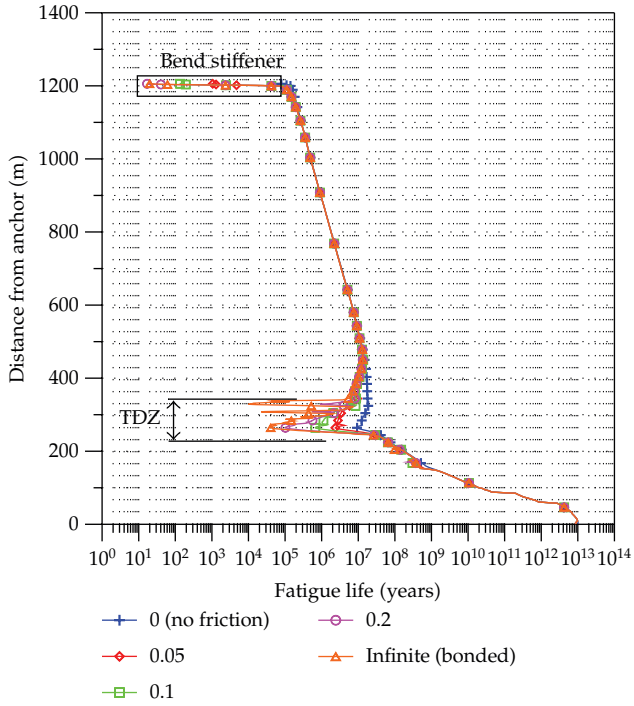

Figure 11: Fatigue life in the inner armor along the flexible pipe: effect of different coefficients of friction.

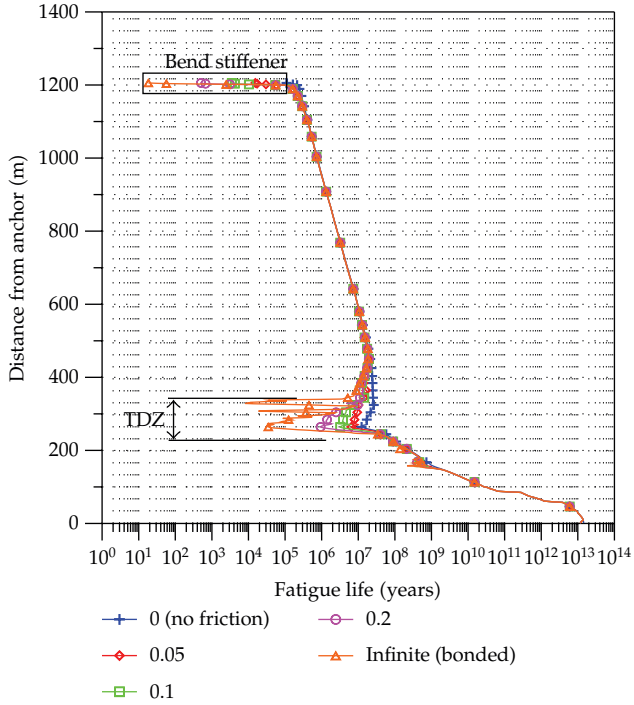

Figure 12: Fatigue life in the outer armor along the flexible pipe: effect of different coefficients of friction.

Table 3: Fatigue life: effect of different friction coefficients.

Friction coefficient	Fatigue life (years)		
	Inner armor	Outer armor	Flexible riser
0.00 (no friction)	77387	109173	77387
0.05	1054	15384	1054
0.10	135	3511	135
0.20	19	503	19
Infinite (bonded)	19	19	19

Table 4: Fatigue life: effect of the number of wires analyzed.

Number of wires	Fatigue life (years)		
	Inner armor	Outer armor	Flexible riser
All	135	3511	135
28	135	3535	135
14	138	3536	138
8	146	3881	146
4	194	3881	194

Kebadze and Kraincanic [20] was adopted:

$$EI_{\text{ns}} = \sum_{i=1}^{n_a} \frac{n_{wi}}{2} \cdot E_i \cdot A_i \cdot r_i^2 \cdot \cos^3(\alpha_i) + EI_{\text{pol}}, \tag{3.1}$$

where n_a is the number of metallic armors in the pipe, EI_{pol} is the bending stiffness of the polymeric layers, and A is the cross-sectional area of each wire of the tensile armor. In this work, a no-slip bending stiffness of about 2100 kNm^2 was calculated, which is 165 times higher than the full slip bending stiffness.

Considering this new bending stiffness value and the dry *S-N* curve, no fatigue damage was observed in the riser, which confirms the indications presented in the work of Smith et al. [4] and Grealish et al. [10] that fatigue analyses considering a dry annulus condition may lead to quite unconservative results. If a dry annulus condition was assumed for stress calculations and the *S-N* curve of the base case was employed for fatigue computation, the fatigue lives presented in Figure 13 would be achieved. There is no variation of the fatigue lives at the top of the riser, but the TDZ is deeply affected, as lower curvatures are induced in this region.

3.5. Effect of Different Number of Wires

Table 4 shows the fatigue life obtained for the flexible riser if different number of wires were analyzed in the cross-section of the pipe. This table indicates that, in this case, at least 8 equally spaced wires around the cross-section of the pipe should be considered, but, as the fatigue life considerably varies in these wires, as shown in Figure 8, the best approach would be to consider at least half of the wires.

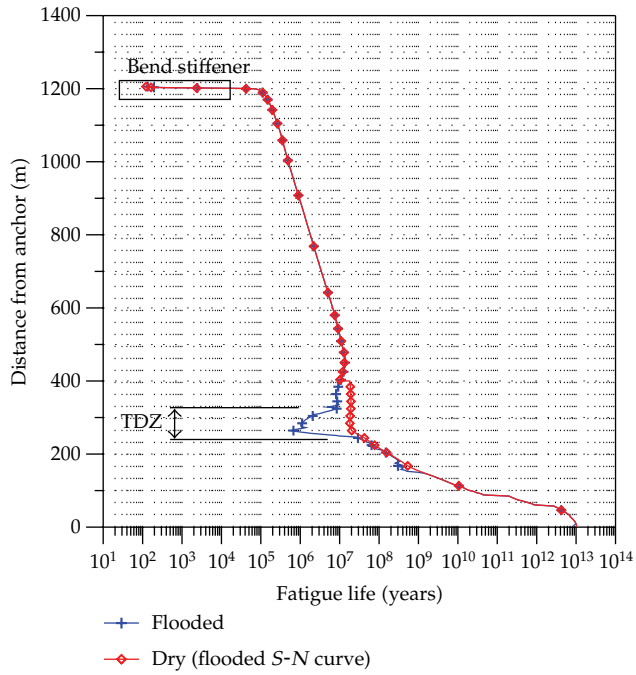

Figure 13: Variation of the fatigue life along the flexible pipe: effect of the annulus conditions (dry values are obtained with the flooded *S-N* curve).

3.6. Effect of Mean Stresses

The *S-N* curve proposed in the base case does not account for mean stress effects, and, therefore, the Goodman correction factor had to be employed. Here, the fatigue life of the wires in the critical cross-section was reevaluated without considering this effect. The results obtained are presented in Figure 14, which indicates that the fatigue life is influenced by the consideration of mean stress effects. The fatigue life of the inner armor is increased from 135 years, to 463 years and the fatigue life of the outer armor also increases from 3511 years to 10200 years.

Hence, a key aspect of the fatigue design of flexible pipes is to account for this effect with the use of correction factors, as indicated here, or of *S-N* curves that directly addresses this effect.

4. Conclusions

The prediction of the fatigue life of flexible pipes is a key issue that must be addressed in order to employ these structures in harsh operational and/or environmental conditions or, furthermore, to possibly extend the use of structures in operation. In comparison to other offshore structures, such as rigid steel pipes, the computation of the fatigue resistance of flexible pipes has two additional difficulties: the global (evaluation of forces and moments) and local (evaluation of stresses) simulations of the bending hysteretic response of these pipes and the calculation of stresses in their armor layers, which is not straightforward. Therefore, the fatigue life assessment of these pipes is not a simple task, which is usually overcome with

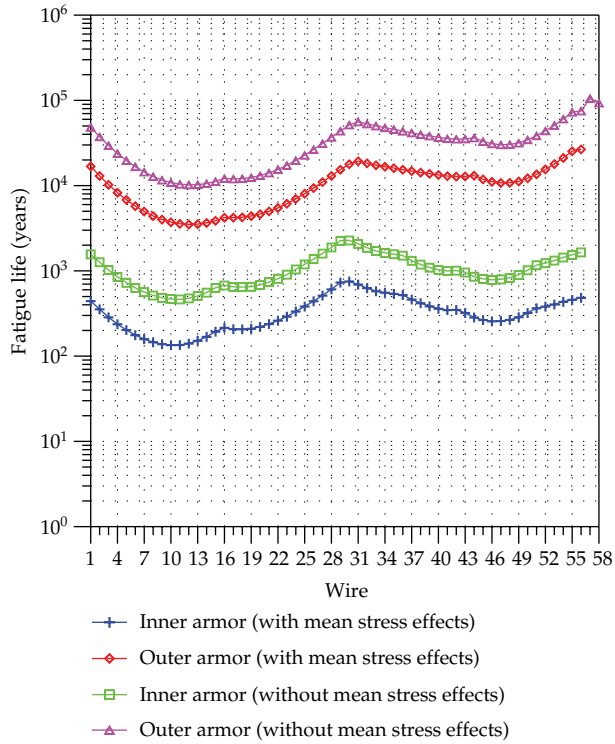

Figure 14: Fatigue life in the wires of the critical cross-section: effect of mean stresses.

theoretical models that assume various simplifying hypotheses leading to quite conservative results. These results may impair their use in the previously stated conditions, and, therefore, less conservative approaches are demanded.

In this work, aiming at reducing the conservatism associated with the fatigue life prediction of flexible pipes, a new theoretical approach was proposed. The main goals of this approach are as follows.

(i) Results from either regular or irregular seastates may be considered.

(ii) Various local analyses may be performed with low computation effort.

(iii) The fatigue computation is based on the analysis of time histories of stresses generated from the time histories of tensions and bending moments (or curvatures) calculated for each seastate in the global analyses. Therefore, the approach directly encompasses dynamic tension variations, and no additional hypotheses on phasing between tensions and curvatures are necessary.

(iv) The possibility of considering either dry or flooded annulus conditions.

(v) The simulation of the bending hysteretic response of flexible pipes in their local analyses in order to generate less conservative time histories of stresses.

(vi) Easy computation of the fatigue life in all wires along the flexible pipe. Moreover, fatigue damage is accumulated at each analyzed point in these wires using rainflow counting techniques, adequate *S-N* curves, and the Palmgren-Miner rule.

A study on the fatigue response of a 6″ flexible riser was carried out using this approach. The fatigue life computation of the riser was based on tensions and moments

calculated with a global FE model that did not consider its bending hysteretic behavior, as, usually, programs devoted to perform global analyses of flexible pipes do not handle this issue.

The results obtained showed two critical regions: the top of the riser including the bend stiffener; and the touchdown zone. The critical cross-sections, however, were located at the top of the riser. In all analyses, the fatigue response of the flexible riser was governed by the resistance of the inner tensile armor wires, as stresses induced by friction with adjacent layers are higher in these wires and these stresses have the highest amplitudes.

Aiming at evaluating the effect of friction on the fatigue response of the riser, fatigue analyses considering different coefficients of friction were conducted. These analyses showed that the choice of the coefficient of friction and the simulation of the hysteretic response of the riser strongly affect its fatigue life. The analysis with no friction presented values much higher than the analysis with a low friction coefficient (0.05) and, therefore, is quite unconservative. However, the calculation of forces and moments with the lower bending stiffness of the pipe (highest possible curvatures) followed by the stress computation considering that the wires are prevented from sliding (fully bonded response and maximum stresses) indicated a fatigue life much lower than intermediate values obtained with friction coefficients of 0.05 or 0.10. This approach is thereby quite conservative. The suggested approach is, consequently, to consider friction coefficients between 0.05 and 0.10 and calculate the fatigue life with the simulation of the hysteretic response, at least, in the local analyses or, ideally, in the local and, if possible, global analyses.

This study also indicated that the annulus condition was of fundamental importance. The assumption of a dry annulus, despite the higher stresses obtained in the TDZ compared to the flooded condition, implicates the use of benefic *S-N* curves which may result in a quite unconservative value, as the fatigue damage is deeply affected by the parameters of these curves. Moreover, the fatigue computation has to consider several wires around the cross-section of the pipe, because the fatigue life significantly varies from wire to wire. Finally, mean stress effects have to be considered directly in the *S-N* curve or through correction factors as it also affects the fatigue computation.

To sum up, it is authors' belief that the results presented here serve as a basis to better understand the fatigue response of typical flexible pipes. However, much remains to be done in this area, as, for instance, in this study, the hysteretic response was not considered in the global analyses, and this is a source of conservatism that can be diminished by adapting global FE models to account for this type of responses; there are doubts regarding the friction coefficients and local models for computing the bending and combined (bending and axisymmetric) responses of flexible pipes, and, consequently, experimental tests are needed in order to validate these models, and experimental tests have also to be performed in order to calibrate the whole proposed approach.

Acknowledgment

Authors from COPPE/UFRJ would like to thank Petrobras for allowing the publication of this work.

References

[1] API, *Recommended Practice for Flexible Pipe, API RP 17B*, American Petroleum Institute, New York, NY, USA, 3rd edition, 2002.

[2] D. de La Cour, C. Kristensen, and N. J. R. Nielsen, "Managing fatigue in deepwater flexible risers," in *Proceedings of the Offshore Technology Conference*, Houston, Tex, USA, 2008.
[3] F. Bectarte, P. Secher, and A. Felix-Henry, "Qualification testing of flexible pipes for 3000 m water depth," in *Proceedings of the Offshore Technology Conference*, Houston, Tex, USA, 2011.
[4] R. J. Smith, P. J. O'Brien, T. O'Sulllivan, and C. Weibe, "Fatigue analysis of unbonded flexible risers with irregular seas and hysteresis," in *Proceedings of the Offshore Technology Conference*, Houston, Tex, USA, 2007.
[5] C. A. D. Lemos, F. J. M. Sousa, and J. R. M. Sousa, "Flexible riser fatigue re-evaluation to extend the service life," in *Proceedings of the 27th International Conference on Offshore Mechanics and Arctic Engineering*, pp. 601–606, Estoril, June 2008.
[6] Y. Zhang, B. Chen, L. Qiu, T. Hill, and M. Case, "State of the art analytical tools improve optimization of unbonded flexible pipes for deepwater environments," in *Proceedings of the Offshore Technology Conference*, Houston, Tex, USA, 2003.
[7] J. J. Feret and C. L. Bournazel, "Evaluation of flexible pipes' life expectancy under dynamic conditions".
[8] R. J. Smith, V. Stoica, and P. J. O'Brien, "Fatigue design of flexible risers with a non-dry annulus".
[9] Z. Tan, P. Quiggin, and T. Sheldrake, "Time domain simulation of the 3D bending hysteresis behaviour of an unbonded flexible riser," in *Proceedings of the 26th International Conference on Offshore Mechanics and Arctic Engineering*, pp. 307–314, San Diego, Calif, USA, June 2007.
[10] F. Grealish, R. Smith, and J. Zimmerman, "New industry guidelines for fatigue analysis of unbonded flexible risers," in *Proceedings of the Offshore Technology Conference*, Houston, Tex, USA, 2006.
[11] S. K. Chakrabarti, *Handbook of Offshore Engineering*, Elsevier, Oxford, UK, 2005.
[12] L. V. S. Sagrilo, E. C. Prates de Lima, and A. Papaleo, "A joint probability model for environmental parameters," *Journal of Offshore Mechanics and Arctic Engineering*, vol. 133, no. 3, Article ID 031605, 7 pages, 2011.
[13] N. D. P. Barltrop, *Floating Structures: A Guide for Design and Analysis*, The Centre for Marine and Petroleum Technology (CMPT), England, UK, 1998.
[14] F. J. M. de Sousa, J. R. M. de Sousa, M. Q. Siqueira, L. V. S. Sagrilo, and C. A. D. Lemos, "A methodology to evaluate the fatigue life of flexible pipes," in *Proceedings of the Rio Pipeline Conference & Exposition*, Rio de Janeiro, Brazil, 2009, IBP1230_09.
[15] J. M. Sheehan, F. W. Grealish, R. J. Smith, and A. M. Harte, "Characterisation of the wave environment in the fatigue analysis of flexible risers," in *Proceedings of the 24th International Conference on Offshore Mechanics and Arctic Engineering (OMAE '05)*, pp. 997–1006, Halkidiki, Greece, June 2005.
[16] J. A. Witz, "A case study in the cross-section analysis of flexible risers," *Marine Structures*, vol. 9, no. 9, pp. 885–904, 1996.
[17] L. M. B. Troina, M. M. Mourelle, M. Brack, J. R. M. de Sousa, and M. Q. de Siqueira, "A strategy for flexible riser analysis focused on compressive failure mode," in *Proceedings of the 14th Deep Offshore Technology*, New Orleans, La, USA, 2002.
[18] S. Saevik, "Theoretical and experimental studies of stresses in flexible pipes," *Computers & Structures*, vol. 89, pp. 2273–2291, 2011.
[19] S. Berge, A. Engseth, I. Fylling et al., "Handbook on design and operation of flexible pipes," Tech. Rep. STF70 A92006, FPS 2000, Flexible Risers and Pipes, NTNF Research Program, Stavanger, Norway, 1992.
[20] E. Kebadze and I. Kraincanic, "Non-linear bending behaviour of offshore flexible pipes," in *Proceedings of the 9th International Offshore and Polar Engineering Conference*, vol. 2, pp. 226–233, Brest, France, 1999.
[21] J. R. M. de Sousa, C. Magluta, N. Roitman, G. B. Ellwanger, E. C. P. Lima, and A. Papaleo, "On the response of flexible risers to loads imposed by hydraulic collars," *Applied Ocean Research*, vol. 31, no. 3, pp. 157–170, 2009.
[22] I. Fylling and A. Bech, "Effects of internal friction and torque stiffness on the global behavior of flexible risers and umbilicals," in *Proceedings of the 10th International Conference On Offshore Mechanics and Arctic Engineering*, Stavanger, Norway, 1991.
[23] P. Estrier, "Updated method for the determination of the service life of flexible risers".
[24] C. M. Larsen, "Flexible riser analysis—comparison of results from computer programs," *Marine Structures*, vol. 5, no. 2-3, pp. 103–119, 1992.
[25] M. M. Mourelle, E. C. Gonzalez, and B. P. Jacob, "ANFLEX—computational system for flexible and rigid riser analysis," in *Proceedings of the 9th International Symposium on Offshore Engineering (COPPE/UFRJ)*, Rio de Janeiro, Brazil, 1995.

[26] Petrobras, "Metocean data—campos basin Rev 0," Tech. Rep. I-ET-3000.00-1000-941-PPC-001, Petrobras Research and Development Center, Rio de Janeiro, Brazil, 1999.
[27] DNV, "Fatigue Design of Offshore Steel Structures," Recommended Practice DNV-RP-C203, Høvik, 2005.